Supplementary Materials for
SNAREs controlling vesicular release of BDNF and development of callosal axons

SUPPLEMENTAL FIGURE LEGENDS

Figure S1 (Related to Main Figures 1-6)

(A-D) Cultured cortical neurons were infected at 5 days *in vitro* (DIV5) with lentiviruses that drive BDNF-pHluorin under the control of either synapsin (Syn) or ubiquitin (Ub) promoter. Each virus was titrated to achieve different levels of expression (100% corresponds to undiluted stock). All experiments were performed at DIV15.

(A) Schematic diagrams of lentivirus shuttle vectors.

(B) Subcellular localization of vesicles carrying BDNF-pHluorin was assessed by confocal microscopy. Neurons were stained with antibodies to GFP (green, as a probe for BDNF-pHluorin), an axonal marker, SMI312 (red), and a somato-dendritic marker, MAP2 (blue). Representative low- and high-magnification images are shown. Scale bars apply to all experimental conditions.

(C) Total cell homogenates were probed by immunoblotting with an antibody to BDNF, which recognizes both the endogenous BDNF and BDNF-pHluorin (GFP; P=pro form; M=mature form). On the right side of the gel, different amounts of recombinant human BDNF were loaded as standards.

(D) Quantitative immunoblot analysis of expression of native BDNF and BDNF-pHluorin. n = 3 cultures for each condition.

(E) Subcellular distribution of vesicles carrying BDNF-pHluorin relative to markers of various organelles. Cultures were uniformly infected at DIV5 with undiluted lentiviruses that drive the expression of BDNF-pHluorin under the control of the Ub promoter. Imaging was performed following staining with antibodies to GFP (green, as a probe for BDNF-pHluorin), indicated vesicular markers (all shown in red), and MAP2 (blue). Representative images illustrate co-localization of BDNF-pHluorin with secretogranin2 and its segregation from synapsin1-positive SVs and TfR-positive recycling endosomes. Last column (on the right) shows images of wildtype neurons that were stained with antibodies to SMI312 (green) and secretogranin2.

(F) Averaged densities of vesicles with detectable BDNF-pHluorin along MAP2-positive dendrites and SMI312-positive axons. n = 9 neurons/group.

(G) Quantitative analysis of co-localization of BDNF-pHluorin with indicated vesicular proteins in neuronal processes. $n \geq 10$ neurons/group.

(H-J) Assessment of TrkB receptor phosphorylation and trafficking. DIV5 neurons were uniformly infected with lentiviruses that express BDNF-pHluorin, BDNF-GFP or NGF-pHluorin under the control of the Ub promoter. Experiments were performed at DIV15.

(H) Confocal imaging was carried out following labeling with antibodies to TrkB (red), GFP (green, as a probe for neurotrophin fusion proteins), and MAP2. Typical low- and high-magnification images are displayed. Scale bars apply to all sets.

(I) Total cell homogenates were probed by immunoblotting with antibodies to TrkB, phosphorylated form of TrkB, and βTubulin (as a loading standard).

(J) Left: Quantitative immunoblot analysis of TrkB expression levels, shown as a ratio of TrkB to βTubulin. Right: Averaged fractions of phosphorylated TrkB in the entire receptor pool. n = 3 cultures/group. Note a selective down-regulation of total TrkB levels and augmentation of receptor phosphorylation by BDNF fusion proteins.

In this and following figures, data are plotted as Mean ± S.E.M., unless specified. * denotes $p<0.05$ (defined by t-test or ANOVA).

Figure S2 (Related to Main Figures 1-6)

Cortical cultures were uniformly infected with indicated lentiviruses at DIV5 and analyzed by TIRF or conventional confocal microscopy at DIV15. All genetically-encoded fluorescent proteins were expressed under the control of the Ub promoter.

(A-G) Live neurons expressing BDNF-pHluorin were monitored under different physiological conditions. All quantifications were performed using image frames of fixed sizes that were collected in time-lapse mode with 100x PlanApo TIRF objective.

(A) Images of a region marked by a box in the wide DIC field show BDNF-pHluorin fluorescence before stimulation (Basal), during depolarization with KCl (50 mM), and following de-acidification of vesicle lumens with ammonium chloride (NH_4Cl, 50 mM). Sites of activity-dependent exocytosis are marked by yellow boxes.

(B-D) Frequencies of BDNF vesicle fusion were plotted as a function of time (10 second bin) under the normal conditions and during stimulation with 50 mM of KCl (panel **B**, green box marks the time-course of calcium rise as determined in identical settings with GCaMP3), 100 Hz action potential trains (APs, panel **C**), and GABA receptor blocker, PTX (100 μM), which promotes synaptic excitation (panel **D**).

(E) Probabilities of fusion (P_f) per minute are plotted as EN/IP ratios. Note that evoked fusion events are virtually undetectable in the presence of the membrane-impermeable hydrophilic quencher, bromophenol blue (BPB).

(F) P_f values were normalized to P_f of neurons that were depolarized with KCl.

(G) Analysis of calcium-dependence of exocytosis. Neurons were stimulated with KCl in the normal NRS solution (2 mM extracellular calcium), calcium-free NRS, or in the presence of calcium channel and NMDA receptor blockers, $CdCl_2$ (100 μM), Nifedipine (50 μM) and APV (50 μM).

(H-J) Comparative analysis of exocytosis of vesicles carrying BDNF-pHluorin and recycling endosomes (REs) that were tagged with TfR-pHluorin.

(H) Representative images show TfR-pHluorin fluorescence in dendrites of DIV15 neurons before and during KCl-induced depolarization.

(I and **J)** Mean EN and P_f before, during and after depolarization. Note that, unlike BDNF vesicles, REs exhibit robust exocytosis in the absence of external stimulation. For all quantifications, $n \geq 10$/group.

(K) Schematic representation of lentivirus shuttle vectors encoding fluorescent reporters of SVs and postsynaptic spines, tdTomato-SV2A and EBFP2-Homer1c.

(L) Neurons carrying tdTomato-SV2A (red) or EBFP2-Homer1c (blue) were stained for native synapsin1 (green) or PSD95 (red). Note that fluorescent tracers do not aggregate and overlap with endogenous synaptic proteins. A typical kymograph from triple time-lapse imaging of co-expressed BDNF-GFP, tdTomato-SV2A and EBFP2-Homer1c is shown in **Figure 1A1**.

(M and **N**) BDNF is released from both synaptic and extra-synaptic sites. BDNF-pHluorin was co-expressed and simultaneously imaged in TIRF mode with tdTomato-SV2A and EBFP2-Homer1c.

(M) Typical images illustrate the distribution of sites of KCl-induced exocytosis of BDNF vesicles (boxed in enlarged panels) relative to SV2A-positive presynaptic terminals.

(N) Quantifications of overlap of BDNF release sites with synaptic reporters. Neurons were transiently stimulated with KCl (50 mM, 2 minutes), PTX (100 μM, 2 minutes) or action potentials applied for 30 seconds at 10 and 100Hz. n = 3-5/group.

Figure S3 (Related to Main Figures 2-6)

(A-C) Distribution of intracellular peptidergic vesicles in SNARE-deficient neurons.

(A) Representative confocal images of wildtype DIV15 neurons and neurons carrying TeNT that were stained with antibodies to secretogranin2 (Sec2, red), SMI312 (green), and MAP2 (blue). Arrows mark SMI312-positive/MAP2-negative axons. A uniform infection protocol was used.

(B) Averaged densities of Sec2-positive vesicles in dendrites and axons of control and TeNT-expressing neurons. *n* = 10 neurons/group.

(C) Cultures were sparsely infected (as described below) with lentiviruses expressing BDNF-pHluorin and either TeNT or shRNAs against Syb2, SNAP25 and SNAP47 (KD). Infected neurons were stained for GFP (green, as a probe for reporter-positive vesicles) and MAP2 (blue). Representative low- and high-magnification confocal images show that, under all conditions, BDNF vesicles are distributed throughout the somas and processes.

(D-H) An experimental system for studies of cell-autonomous effects of SNARE loss of function.

(D) A graphic outline of culture preparation. Neurons were treated immediately after plating with a lentivirus encoding mCherry alone or together with other viruses of interest. Infected cells were then mixed at DIV1 with wildtype neurons at a 1:20 ratio, and these cultures were examined after DIV15.

(E) Schematic representation of lentivirus shuttle vectors expressing mCherry, GCaMP3 and TeNT.

(F) Typical DIC and fluorescent images of different magnification show somas, dendrites and axons of live mCherry-tagged neurons surrounded by non-infected cells (marked by asterisks in wide-field images).

(G) DIC and fluorescent images of live neurons sparsely co-expressing GCaMP3 and TeNT. Infected cells were monitored in time lapse mode before (Basal) and during augmentation of synaptic excitation with PTX (100 μM). Asterisks mark the somas of non-infected cells.

(H) Sample traces reflecting changes in intracellular calcium levels in indicated conditions, plotted as a ΔF/F0 ratio of GCaMP3 fluorescence. Note that neurons sparsely co-expressing GCaMP3 and TeNT in mixed cultures exhibit robust responses to PTX (100 μM), whereas uniform infection with TeNT completely abolishes these responses.

Figure S4 (Related to Main Figure 3)

Neurons were uniformly infected at DIV5 with lentiviruses encoding BDNF-pHluorin and two different shRNAs that target Syb/VAMP isoforms 1, 2 and 3 (target sequences are listed in **Table S1)**. Cultures were examined at DIV15-17 by immunoblotting and live TIRF imaging.

(A) Schematic diagrams of lentivirus vectors.

(B) Quantitative immunoblot analysis of pro- (P) and mature (M) BDNF levels was performed using antibodies to BDNF and βTubulin (as a loading standard). *n* = 6 control and Syb/VAMP-deficient cultures (examined in duplicates, KD = shRNA-mediated knockdown). Representative blots are shown in **Figure 3C.** Note a selective accumulation of mature BDNF in neurons carrying shRNAs against Syb/VAMP2.

(C) TIRF microscopy analysis of BDNF-pHluorin exocytosis. Graphs show averaged numbers of depolarization-induced fusion events (EN) and densities of intracellular reporter-positive vesicles counted after de-acidification with 50 mM of NH_4Cl (IP). Control, *n* = 7; Syb1 KD, *n* = 6; Syb2 KD, *n* = 7; Syb3 KD, *n* = 7. See also **Figure 2D-F.**

(D) Representative confocal images of wildtype neurons and neurons carrying shRNAs against Syb2 that were labeled at DIV15 with antibodies to MAP2 (blue) and Syb2 (green). Note a lack of cytotoxicity and a loss of Syb2 immunoreactivity upon KD.

(E and **F)** Cultures uniformly expressing indicated shRNAs alone (KD) or together with rescue cDNAs were examined by immunoblotting for native Syb2 and βTubulin.

(G) Quantitative immunoblot analysis of mature BDNF levels in wildtype, Syb2 KD and Syb2 KD + rescue neurons. *n* = 3 cultures/group, analyzed in duplicates using a uniform virus infection protocol.

(H-J) Subcellular localization of native Syb2.

(H) Wildtype DIV15 neurons were examined by confocal microscopy following immunostaining with antibodies to Syb2 (red), SMI312, synapsin1 and PSD95 (all in green), and MAP2 (blue). In each panel, typical images are shown at 3 different magnifications. Scale bars apply to all sets.

(I) Cultures were sparsely infected with a lentivirus that drives the expression of BDNF-pHluorin under the control of the Ub promoter. Neurons were examined by confocal microscopy at DIV15 following immunostaining with antibodies to Syb2 (red), GFP (green, as a probe for BDNF-pHluorin), MAP2, synapsin1 and PSD95 (all in blue). Scale bars apply to all sets.

(J) Quantitative analysis of co-localization of indicated proteins in wildtype neurons (images not displayed) and neurons expressing BDNF-pHluorin. *n* = 9 neurons/group.

<u>Figure S5</u> (Related to Main Figure 4)

(A and **B)** Cultures were uniformly infected at DIV5 with lentiviruses encoding BDNF-pHluorin and two different shRNAs that target SNAP isoforms 23, 25, 29 and 49 (target sequences are listed in **Table S1**). Neurons were examined at DIV15 by immunoblotting and live TIRF imaging.

(A) Quantitative immunoblot analysis of pro- (P) and mature (M) BDNF-pHluorin and native BDNF levels was performed using antibodies to BDNF and βTubulin (as a loading standard). *n* = 3 cultures (examined in duplicates, KD = shRNA-mediated knockdown). Note a selective accumulation of mature BDNF forms in neurons carrying shRNAs against SNAP25.

(B) TIRF microscopy analysis of BDNF-pHluorin exocytosis. Graphs show averaged numbers of depolarization-induced fusion events (EN) and densities of intracellular reporter-positive vesicles counted after de-acidification with 50 mM of NH_4Cl (IP). Control, *n* = 10; SNAP23 KD, *n* = 8; SNAP25 KD, *n* = 8; SNAP29 KD, *n* = 7; SNAP47 KD, *n* = 8. See also **Figure 4B-D.**

(C) Wildtype DIV15 neurons and neurons carrying shRNAs against SNAP25 or SNAP47 were labeled with antibodies to MAP2 (blue) and corresponding SNAPs (green). Typical confocal images demonstrate a lack of cytotoxicity and a loss of SNAP25/47 immunoreactivity upon KD.

(D) Neurons were uniformly infected with lentiviruses driving the expression of indicated shRNAs alone (KD) or together with rescue cDNA, and then examined by immunoblotting for native SNAP25, SNAP47 and βTubulin.

(E) Quantitative immunoblot analysis of mature BDNF levels in control, SNAP25 KD and SNAP25 KD + rescue neurons. *n* = 3 cultures/condition, analyzed in duplicates using a uniform virus infection protocol.

(F-H) Subcellular localization of native SNAPs. Cultures were sparsely infected with a lentivirus that drives the expression of BDNF-pHluorin under the control of the Ub promoter. Neurons were examined by confocal microscopy at DIV15 following immunostaining with antibodies to SNAP25/47 (both in red, panels **F** and **G**, respectively), GFP (green, as a probe for BDNF-pHluorin), MAP2, synapsin1 and PSD95 (all in blue). In each panel, typical images are shown at 3 different magnifications. Scale bars apply to all sets.

(H) Quantitative analysis of co-localization of indicated proteins in wildtype neurons and neurons expressing BDNF-pHluorin. *n* = 9 neurons/group.

Figure S6 (Related to Main Figure 4)

Kinetics of depolarization-induced exocytosis of BDNF-pHluorin was assessed by TIRF imaging in somas, dendrites and axons of sparsely infected neurons tagged with mCherry.

(A and **B)** Examples of full vesicle collapse (FC) and partial fusion (PF) in wildtype neurons. Panels illustrate decay of BDNF-pHluorin signal in two isolated sites (**A**, frames were collected every 5 seconds, arrow marks the onset of fusion) and corresponding traces of reporter fluorescence monitored in time-lapse mode (**B**, the onsets of exocytosis were digitally re-synchronized).

(C) Dual-exponential fits of averaged BDNF-pHluorin responses whose onsets and amplitudes were synchronized using a custom-made script integrated in the Origin8 software. Data were sampled from somas and dendrites of single wildtype neurons. Events were either pooled together (All) or segregated based on visual inspection followed by curve fitting. Time constants of decay are shown in inserts (e.g. 8/34 are numerical values of Tau1 and Tau2, respectively). FC: *EN*=34; PF: *EN*=149

(D) Representative images of fusion events (top panels) with corresponding kymographs (bottom panels, scale bars apply to all panels) detected in somato-dendritic domains of control neurons, and neurons expressing SNAP47 shRNA alone or with rescue cDNA.

(E) Averaged percentages of FC and PF-type fusion events in axonal and somato-dendritic compartments of control neurons.

(F) Fractions of FC and PF-type fusion events in axonal and somato-dendritic compartments of SNAP47-deficient neurons, plotted as % of control. *N*=9-10 neurons/group.

Figure S7 (Related to Main Figure 5)

DIV5 cultures were uniformly infected with lentiviruses expressing TeNT or shRNA against SNAP47. At DIV15, neurons were stained with antibodies to native synaptic proteins and subsequently examined by confocal microscopy.

(A and **B)** Typical low- and high-magnification images of neurons labeled for MAP2 (blue), synapsin1 (green) and markers of glutamatergic and GABAergic terminals, VGlut1 and VGAT (red in panels **A** and **B**, respectively).

(C) Quantitative analysis of the distribution of synapsin1, VGlut1 and VGAT-positive synapses. Average values show puncta densities along dendrites as a function of distance from cell bodies (5 μm bin). n = 15 neurons/group.

Figure S8 (Related to Main Figures 6 and 7)

(A and **B)** Subcellular distribution of SNAREs in differentiating cortical neurons in culture.

(A) Representative confocal images of wildtype DIV6 and DIV15 neurons that were labeled with antibodies to synapsin1 (red) and MAP2 (blue). Note a difference in the distribution of synapsin1 along axons (MAP2-negative processes).

(B) Wildtype DIV6 neurons were labeled for native Syb2, SNAP25 or SNAP47 (all in red) together with MAP2 (blue) and axonal markers, Tuj1 or SMI312 (both in green). Arrows mark Tuj1 and SMI312-positive axons.

(C) SNAP47 is abundant in callosal axons *in vivo.* Cortical sections were prepared from brains of P30 mice and stained with antibodies to SNAP47 (red) and MAP2 (magenta). Typical confocal images of corpus callosum and somato-sensory cortex (SSC) are shown. White arrow marks callosal axons.

(D and **E)** E15.5 embryos were *in utero* electroporated into one cortical hemisphere with mVenus tracer together with control shuttle vector or vectors encoding SNAP47 shRNA/rescue constructs.

(D) Images of the ipsi-lateral cortex in brain sections show mVenus-tagged neurons (top) and fragments of their dendrites with characteristic postsynaptic spines at P21.

(E) Quantifications of spine densities in control and SNAP47-deficient neurons. *n* = 5 mice/group.

(F and **G)** E15.5 embryos were *in utero* electroporated into one cortical hemisphere with vectors driving the expression of mVenus and shRNAs against SNAP47, BDNF or BDNF receptor, TrkB. Axon branching was examined *in vivo* at postnatal day 21. Graphs show averaged mVenus fluorescence intensities across the contralateral column. Signal was normalized to the white matter (WM, 100% defined as the maximum value). Control, *n* = 11 mice; SNAP47 KD, *n* = 8 mice; SNAP47 KD + Rescue, *n* = 5 mice. BDNF KD, *n* = 3 mice; TrkB KD, *n* = 8 mice.

Movies.

All movies were generated from time-lapse TIRF image stacks sampled at 1 Hz. The speed is 60x of actual acquisition speed. Each movie illustrates exocytosis of BDNF-pHluorin during transient depolarization with KCl (2 minutes) followed by de-acidification of internal vesicles with the buffer containing ammonium chloride. Panels are comprised of representative stacks used for quantitative analysis of EN, IP and P_f with isolated regions of detectable exocytosis (ROI) shown as inserts. Movies of BDNF exocytosis in SNARE-deficient neurons can be provided upon request.

Movie SM1 (Related to Main Figures 1-4)
Evoked exocytosis of BDNF-pHluorin followed by vesicle de-acidification in mature DIV15 neuron.

Movie SM2 (Related to Main Figures 2-4)
Evoked exocytosis of BDNF-pHluorin followed by vesicle de-acidification in soma and dendrites of mCherry-tagged DIV15 neuron in sparsely-infected culture.

Movie SM3 (Related to Main Figures 2-5)
Evoked exocytosis of BDNF-pHluorin followed by vesicle de-acidification in axons of mCherry-tagged DIV15 neuron in sparsely-infected culture.

Movie SM4 (Related to Main Figure 6)
Evoked exocytosis of BDNF-pHluorin followed by vesicle de-acidification in axons of immature mCherry-tagged DIV6 neuron in sparsely-infected culture.

Table S1. Expression vectors (Related to Main Figures 1-7)

Expression Vector	Origin	Aminoacids/Target sequence	Promoter	NCBI AN/Reference
FGW (Lentiviruses)				(Sando et al., 2012)
BDNF-GFP	Mouse	1-249 (full-length BDNF)	Ub	(Brigadski et al., 2005)
BDNF-pHluorin	Mouse	1-249 (full-length BDNF)	Ub	(Matsuda et al., 2009)
BDNF-pHluorin	Mouse	1-249 (full-length BDNF)	Syn	
NGF-pHluorin	Mouse	1-241 (full-length NGF)	Ub	NM_001112698.2
SyP-pHluroin	Mouse	1-314 (full-length Synaptophysin)	Ub	(Peng et al., 2012)
TfR-pHluroin		1-760 (full-length TfR)	Ub	(Wang et al., 2008)
tdTomato-SV2A	Rat	1-742 (full-length SV2A)	Ub	(Chang and Sudhof, 2009)
EBFP2-Homer1c	Rat	1-366 (full-length Homer1)	Ub	(Charrier et al., 2012)
GCaMP3	Synt.	1-450 (full-length GCAMP3)	Ub	HM143847
mCherry	Synt.	1-236 (full-length mCherry)	Syn	
TeNT LC	Synt.	1-455 (light chain TeNT)	Syn	L19522.1
Syb1 KD (1)	Mouse	GGACATCATGCGTGTGAAT	H1	NM_009496.3
Syb1 KD (2)	Mouse	GTGCCATCATCGTGGTAGT	H1	NM_009496.3
Syb2 KD (2)	Mouse	GTGCAGCCAAGCTCAAGCG	H1	NM_009497.3
Syb2 KD (3)	Mouse	GTGGACATCATGAGGGTGA	H1	NM_009497.3
Syb3 * KD (1)	Mouse	GATGTGGGCGATAGGGATC	H1	NM_009498.4
Syb3 KD (3)	Mouse	GGTGTTAGAAAGAGACCAG	H1	NM_009498.4
SNAP23 KD (1)	Mouse	GGAAAGAACTATAAGGCAA	H1	NM_009222.3
SNAP23 KD (2)	Mouse	CTGGAAAGCACAAGGAGAA	H1	NM_009222.3
SNAP25 KD (1)	Mouse	GCGAACAACTGGAACGCAT	H1	NM_011428.3
SNAP25 KD (2)	Mouse	GCCATATGGCTCTAGACAT	H1	NM_011428.3
SNAP25 KD (3)	Mouse	GGTTATGTTGGATGAGCAA	H1	NM_011428.3
SNAP29 KD (1)	Mouse	GCAGATTGAAAGAAGCCAT	H1	NM_023348.4
SNAP29 KD (2)	Mouse	CAGAGAAGATGGTAGACAA	H1	NM_023348.4
SNAP47 KD (1)	Mouse	GCATACGCCAGCGCTTCAT	H1	NM_144521.2
SNAP47 KD (2)	Mouse	CGATCACAGTCCTGGAGAA	H1	NM_144521.2
BDNF KD (1)	Mouse	GGTGATGCTCAGCAGTCAA	H1	NM_001048139.1
BDNF KD (2)	Mouse	CCCGGTATCCAAAGGCCAA	H1	NM_001048139.1
BDNF KD (3)	Mouse	GCCGAACTACCCAATCGTA	H1	NM_001048139.1
TrkB KD (1)	Mouse	GCGTTGACCCGGAGAACAT	H1	NM_001025074.1
TrkB KD (2)	Mouse	GTACTGGGACGTTGGGAAT	H1	NM_001025074.1
Syb2 KD/Rescue	Rat	GTGCGGCAAAACTTAAACG **	H1/Syn	NM_012663.2
SNAP25 KD/Rescue	Mouse	GCGAGCAGTTGGAGCGTAT **	H1/Syn	NM_011428.3
SNAP47 KD/Rescue	Mouse	GTATTCGGCAACGGTTCAT **	H1/Syn	NM_144521.2
Syb1-Venus	Mouse	1-118 (full-length Syb1)	Ub	NM_009496.3
Syb2-Venus	Rat	1-116 (full-length Syb2)	Ub	M24105.1
Syb3-Venus	Mouse	1-103 (full-length Syb3)	Ub	NM_009498.4
VAMP4-Venus	Mouse	1-141 (full-length VAMP4)	Ub	AK018344.1
VAMP5-Venus	Mouse	1-102 (full-length VAMP5)	Ub	NM_016872.4
VAMP7-Venus	Mouse	1-220 (full-length VAMP7)	Ub	NM_011515.4
VAMP8-Venus	Mouse	1-101 (full-length VAMP8)	Ub	NM_016794.3
YKT6-Venus	Mouse	1-198 (full-length YKT6)	Ub	NM_019661.4
Sec22b-Venus	Mouse	1-215 (full-length Sec22b)	Ub	NM_011342.4
SNAP23-Venus	Mouse	1-210 (full-length SNAP23)	Ub	NM_009222.3
SNAP25-Venus	Mouse	1-206 (full-length SNAP25)	Ub	NM_011428.3
SNAP29-Venus	Mouse	1-260 (full-length SNAP29)	Ub	NM_023348.4
SNAP47-Venus	Mouse	1-413 (full-length SNAP47)	Ub	NM_144521.2
pSCV2 backbone				
mVenus	Synt.	Full-length monomeric Venus	CAG	(Courchet et al., 2013)

* Syb3 is also known as Cellubrevin. ** Silent mutations that disable RNA interference are shown in red.

Table S2. Synaptic transmission in cultured Syb2, SNAP25- and SNAP47-deficeint cortical neurons (Related to Main Figure 5)

	Mean +/- S.E.M.	*n***	P value***
Evoked EPSC amplitude (nA)			
Control	1.0 +/- 0.2	13	
TeNT	0.13 +/- 0.04	11	<0.001
SNAP47 KD*	1.1 +/- 0.2	13	0.51
SNAP47 KD + Rescue	1.1 +/- 0.02	10	0.64
Evoked IPSC amplitude (nA)			
Control	3.6 +/- 0.4	19	
TeNT	0.05 +/- 0.03	3	<0.001
Syb2 KD*	0.3 +/- 0.1	5	<0.001
SNAP25 KD	2.0 +/- 0.5	12	0.01
SNAP47 KD	3.3 +/- 0.3	14	0.44
SNAP47 KD + Rescue	3.8 +/- 0.6	10	0.68

*KD = shRNA-mediated knock-down.
***n* = total number of neurons analyzed; each synaptic parameter was examined in at least two independent neuronal culture preparations.
*** P values (experimental versus control group).

EXTENDED METHODS

Reagents. The following commercial polyclonal and monoclonal antibodies were used for immunocytochemistry and immunoblotting: anti-BDNF (Santa Cruz, N20, sc-546); anti-Cux1 (Santa Cruz, M-222, sc13024); anti-βTubulin III (Sigma, T2200); anti-SMI312 (Covance, SMI-312R); anti-MAP2 (Sigma, clone HM2, M4403); anti-MAP2 (Millipore, clone AP20, MAB3418); anti-MAP2 (Millipore, AB5622); anti-TrkB (Millipore, 07-225); anti-vGluT1 (Millipore, AB5905); anti-phosphoTrk (Cell Signaling, 4621); anti-GFP (AVES, GFP-1020); anti-SNAP47 (SySy, 111 403); anti-VGAT (SySy, 131 003); anti-Synaptobrevin2 (SySy, 104 211); anti-SNAP25 (SySy, 111 011); anti-Synapsin (SySy, 106 011); anti-SecII (Biodesign International, K5510R); Other antibodies were a kind gift of Dr. Thomas Südhof. Toxins and inhibitors were purchased from Tocris or Sigma and used at the following concentrations: APV (Cat# 01061, 50 μM), CNQX (Cat# 01045, 10 μM), Picrotoxin (Cat# 1128, 100 μM), Tetrodotoxin (Cat# 50809813, 1 μM).

Mice. Wildtype mice of a mixed 129SvJ/C57BL/6J background were used for preparation of neuronal cultures and immunoprecipitations. *In utero* electroporations were performed in wildtype F1-hybrid females resulting of the cross between inbred C57BL/6J and 129SvJ parents. *CamKIIα*:Cre and *R26*$^{\text{floxstop-TeNT}}$ alleles were described previously (Sando et al., 2012; Zhang et al., 2008). Animals were housed and analyzed according to the protocols approved by the IACUC committee.

Plasmid construction. Coding sequences were inserted into previously characterized FGW shuttle vector that contains recombination arms, a flap HIV-1 sequence, a multiple cloning site, and a WRE element (Maximov et al., 2009; Sando et al., 2013; Sando et al., 2012). Expression of cDNAs and shRNAs was driven by the Ubiquitin (Ub, Pol II), Synapsin (Syn, Pol II) and H1 (Pol III) promoters. Knockdown/rescue studies were carried out with vectors containing Syn and H1 promoters in the same backbone. These constructs were used to produce recombinant lentiviruses in HEK293 cells and for *in utero* electroporation

(as plasmid DNA). For TeNT cleavage assays, shuttles driving the expression of GFP-tagged SNAREs and untagged TeNT under the control of the Ub promoter were transiently transfected into HEK293 cells. Sequences encoding BDNF-pHluorin, BDNF-GFP (Venus), SyP-pHluorin and TeNT were described previously (Brigadski et al., 2005; Matsuda et al., 2009; Peng et al., 2012; Sando et al., 2013), and were a kind gift of Dr. Thomas Südhof. To generate pre- and postsynaptic markers with non-overlapping excitation/emission spectra, two well-characterized reporters, EGFP-SV2A and EGFP-Homer1c (Chang and Sudhof, 2009; Charrier et al., 2012) were modified by replacing EGFP with tdTomato and EBFP2, respectively. The appropriate sorting of these markers to synapses was confirmed by co-labeling of mature neurons for native synapsin1 and PSD95. GCaMP3 and mCherry were a kind gift of Dr. Ulrich Mueller. TfR-pHluorin was a kind gift of Dr. Michael Ehlers. All other cDNAs were amplified by PCR using embryonic mouse brain cDNA library as a template.

Design and validation of vectors expressing shRNAs. Synthetic oligonucleotides encoding hairpins were inserted into XhoI/XbaI sites immediately downstream of the H1 promoter. All constructs were verified by sequencing prior to use. shRNAs were initially pre-screened in cultured neurons by lentiviral co-expression with corresponding GFP-tagged cDNAs to meet three criteria, as determined by live GFP imaging, detection of native proteins, and immunostaining for common neuronal and synaptic markers: i) high potency of knock-downs (>90%); ii) lack of cross-reactivity with mRNAs of homologous genes; and iii) lack of cytotoxicity. Validated shRNAs were then co-expressed in duplicates, and the effects of knockdowns on BDNF levels and efficacy of vesicle exocytosis were assessed by immunoblotting and TIRF microscopy. Subsequently, one shRNA per each candidate SNARE was used to generate dual-promoter rescue vectors harboring cDNAs with silent non-coding mutations that disable RNA interference. See **Table S1** below for additional sequence information and NCBI database accession numbers (ANs). Full vector NTI maps can be provided upon request.

TIRF imaging. We chose to image BDNF-pHluorin by TIRF microscopy since no fast readouts for release of native BDNF exist. This method enables monitoring exocytosis with high temporal and spatial resolution, and diminishes artifacts associated with occasional fluctuations of reporter fluorescence in internal vesicles. We used the published protocol (Matsuda et al., 2009) with several modifications. BDNF-pHluorin was introduced into primary neurons in dissociated cultures with low densities of astrocytes (2-3%) to avoid interference from glia that often resides between neurons and glass interface. Our pilot experiments indicated that relatively high BDNF-pHluorin copy numbers per vesicle are necessary for reliable detection of fusion events. To ensure that overexpression does not result in abnormal vesicular sorting, we systematically examined the processing and subcellular distribution of BDNF-pHluorins that were introduced with lentiviruses of various titers and under the control of the ubiquitin (Ub) or synapsin (Syn) promoters of different strength (**Figure S1A**). Neurons were infected at 5 days *in vitro* (DIV5) and analyzed by immunoblotting and immunostaining at DIV15, when they establish polarized morphologies with abundant synaptic connectivity. In all cases, recombinant proteins were cleaved into mature forms, and were sorted into vesicles that enter SMI312-positive axons and MAP2-positive dendrites (**Figure S1B-D**). Further analysis of neurons expressing BDNF-pHluorin from a stronger Ub promoter showed that 70-80% of reporter-containing vesicles were immunoreactive for a native marker of peptigergic vesicles, secretogranin2. In contrast, these organelles were largely segregated from markers of presynaptic boutons, postsynaptic spines, as well as TfR-positive recycling endosomes that are thought to mediate the membrane

insertion of postsynaptic AMPA receptors during long-term potentiation (**Figures S1E** and **S1G**). Lastly, BDNF-pHluorin but not NGF-pHluorin promoted the phosphorylation and degradation of native TrkB receptors without producing apparent changes in receptor localization (**Figure S1H-J**). Taken together, these results suggest that mis-targeting of the reporter was unlikely.

All TIRF imaging studies were performed with a 100x PlanApo TIRF (N.A. 1.49) objective. We calibrated the perfusion system by determining the time-course of KCl-induced calcium rise in neurons carrying GCaMP3. Additional control experiments were performed to ensure that, similar to native BDNF, BDNF-pHluorin is secreted in an activity- and calcium-dependent manner and that observed changes in reporter fluorescence reflect vesicle fusion with the plasma membrane (**Figure S2A-G**). Side-by-side analysis of BDNF-pHluorin, SyP-pHluotin, and TfR-pHluorin revealed drastic differences in spatial and temporal dynamics of exocytosis, which further rules out the possibility of non-specific targeting of reporters into all vesicle types (**Figures 1D-E** and **S2H-J**).

Our strategies for quantitative analysis of exocytosis and data representation were devised to take into consideration the following: i) Desynchronized nature of BDNF release. Because fusion events occur at different times during neuronal excitation, we present event maps and real-time traces that reflect exocytosis in each site; ii) Potential fluctuation in neuron and vesicle density across different experiments. We took this into account by calculating the total numbers of new events (EN) that appear during fixed time intervals, numbers of internal reporter-positive vesicles counted after de-acidification (intracellular pool, IP) and probability of fusion (P_f=EN/IP). We also plot averaged EN as a function of time using 10 second bins, since the frequency of exocytosis is relatively low even during robust stimulation; iii) Potential fluctuation in BDNF-pHluorin expression levels and pH of the bath solution across independent experiments. Both factors affect the peak amplitudes of reporter response during exocytosis ($\Delta F/F0$). We therefore exclusively test the effects of SNARE loss-of-function on EN, IP, P_f and kinetics of decay, and do not compare peak amplitudes.

In live imaging studies with sparsely infected neurons, axons, dendrites and somas were distinguished by mCherry reporter expression. We validated this approach by performing immunostaining of mCherry-tagged neurons with markers of axonal and somato-dendritic compartments, SMI312 and MAP2. To further avoid contamination with events that arise from intermingled processes of neighboring cells, frames for high-resolution TIRF imaging were first selected at low magnification for areas of distal axon segments or somas with proximal dendrites. We did not image distal dendrites since they can be confused with axons. Because TIRF imaging of BDNF-pHluorin can only be performed at high magnification, we were unable to simultaneously monitor exocytosis from the entire surface of a neuron. Thus, raw EN measurements only reflect isolated segments of axons and the total numbers of fusion events per cell are actually larger. Nevertheless, this problem is alleviated by measurements of P_f. It is also essential to note that, during imaging of mixed cultures, many axons of BDNF-pHluorin-expressing neurons were present in each field of view as opposed to axons of single mCherry-tagged neurons. Therefore, EN values calculated in axons and dendrites of individual neurons cannot be summed for direct comparison with values obtained from mixed cultures.

For analysis of vesicle fusion kinetics (**Figure S6**), single traces of BDNF-pHluorin fluorescence were sampled from sparsely infected mCherry-tagged neurons. These traces were digitally re-synchronized using a custom-made script developed in collaboration with the Origin Lab. Consistent with previous work

(Matsuda et al., 2009), we found that BDNF vesicles fuse with the plasma membrane in two modes: full vesicle collapse (FC) and partial fusion (PF) pore opening. PF and FC-type events were segregated using the following criteria: events decaying by >75% within 15 seconds were considered FC. The remaining slowly decaying events were counted as PF. All multi-peak events were excluded from these quantifications. Decay time constants were determined by double-exponential fitting with the following formula: $y = y_0 + A_1e^{-x/t1} + A_2e^{-x/t2}$. In wildtype neurons, ~80% ($p<0.01$) of fusion events resembled PF vesicles that gradually secrete cargo after the onset of exocytosis, resulting in a slow decay of reporter fluorescence (**Figure S6A-C** and **S6E**). KD of SNAP47 only suppressed the PF mode in axons, while the remaining rapidly decaying FC-type events were abolished in all subcellular domains (**Figure S6D-F**). Given the relatively low frequency of FC, it is not surprising that this shift towards PF could not be revealed by our initial quantifications of total EN and P_f in somas and dendrites. On the contrary, KDs of Syb2 and SNAP25 had a tendency to abolish both fusion modes, albeit the small number of events available for quantification precluded us from obtaining sufficient statistical power (data not shown). Therefore, SNAP47 predominantly controls the bulk exocytosis of BDNF in axons, while promoting the full vesicle collapse across somas and processes.

Owning to its many roles in synaptic plasticity, BDNF is widely believed to be secreted at synapses (Edelmann et al., 2014; Park and Poo, 2013). Yet, the experimental evidence supporting this hypothesis is largely based on imaging studies with cultured neurons where overexpressed BDNF-GFP or BDNF-pHluorin were observed to overlap with markers comprised of synaptic proteins fused to mCherry or dsRed (Brigadski et al., 2005; Kolarow et al., 2007; Shinoda et al., 2011). In our hands, all mCherry- and dsRed-tagged synaptic proteins (but not mCherry alone) aggregated in somas, axons and dendrites, suggesting these markers cannot be used for reliable analysis of co-localization (these images can be provided upon request). We detected significant aggregation even when mCherry and dsRed fusions were assembled following strategies that produce satisfactory results with EGFP, Venus, YFP and CFP. We selected tdTomato-SV2A and EBFP2-Homer1c after extensive screening for reliable markers whose excitation/emission spectra do not overlap with BDNF-pHluorin, and confirmed appropriate targeting of these fusions by co-staining neurons with antibodies to other native pre- and postsynaptic proteins (these data can be provided upon request). In fact, our observation that many BDNF release sites are segregated from synapses is not surprising. Indeed, the exocytosis of BDNF does not appear to require compartmentalized active zones and postsynaptic spines, considering that even immature differentiating neurons exhibit a robust release of native BDNF and BDNF-pHluorin in response to excitation (**Figure 6A-C**) (Balkowiec and Katz, 2000; Cheng et al., 2011).

Analysis of axon branching in vitro. Shuttle vectors encoding shRNA without or with rescue cDNA (1 μg/ml) were mixed with 1% Fast Green (Sigma) and pSCV2-mVenus plasmid. These mixtures were injected into the lateral ventricles of E15.5 embryos of time-pregnant mice followed by electroporation as previously described (Courchet et al., 2013). Immediately after electroporation, the cortices were isolated in HBSS supplemented with 1 mM HEPES-NaOH, pH7.4 and glucose and digested with papain (Worthington) and DNase (Sigma). Dissociated cells were plated onto poly-D-Lysine and laminin (Sigma) coated glass coverslips at a density of 35,000-50,000cells/cm^2. Cultures were fixed at DIV5 and the mVenus fluorescence was enhanced by immunostaining for GFP followed by labeling with Alexa488 secondary antibody. Axons and dendrites were distinguished based on characteristic morphology and by

staining with antibodies to axonal and somato-dendritic markers, SMI312 and MAP2. The numbers of axon branches in each isolated neuron were measured using Nikon NIS-elements and Simple Neurite Tracer plugins. Recombinant human BDNF (Sigma) was daily added to the culture medium starting at DIV1 a concentration of 50 ng/ml.

Analysis of axon branching in vivo was performed using published protocols (Courchet et al., 2013). Briefly, E15.5 embryos were electroporated *in utero* with a mixture of plasmids as describe above. At postnatal day 21, mice were anesthetized and sacrificed by terminal perfusion of 4% paraformaldehyde. Brains were post-fixed in 4% PFA for 2 hours at room temperature. 100 μm free-floating coronal slices (including the corpus callosum) were cut with a vibratome VT1200S (Leica). Sections were subsequently blocked and permeabilized in the PBS buffer containing 1% BSA and 0.2 % Triton X-100 followed by treatments with primary and secondary antibodies to enhance the mVenus signal. Nuclei were labeled with Hoechst 33258 (Pierce). Samples were mounted on slides and imaged under a Nikon C2 confocal microscope.

Miscellaneous. For quantitative immunoblot analysis of BDNF levels, intensities of chemiluminescent signals were measured with ImageJ software using calibration curves obtained with synthetic human BDNF (Almone Lab) and mouse brain lysate.

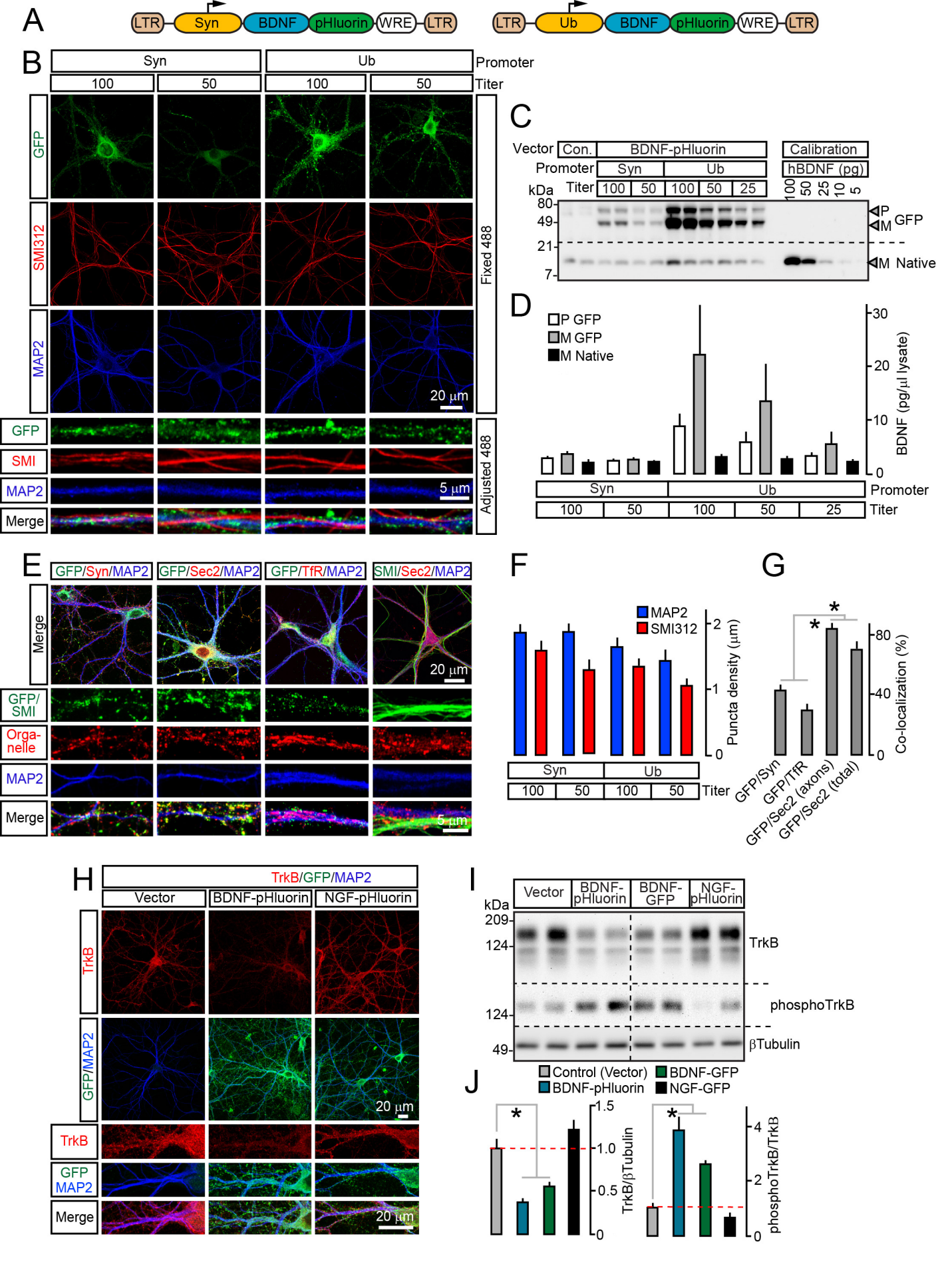

Fig. S1 Shimojo et al

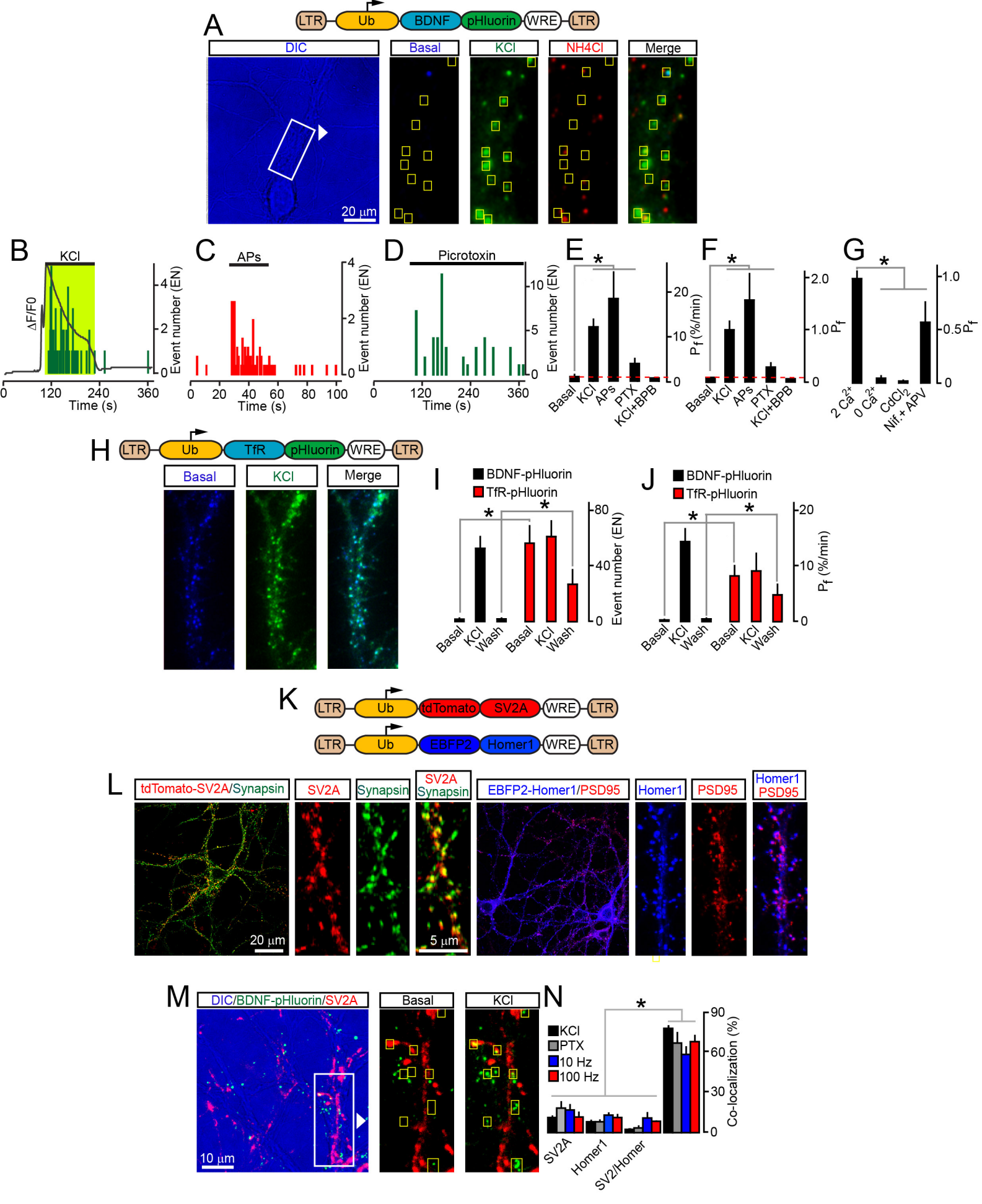

Fig. S2 Shimojo et al

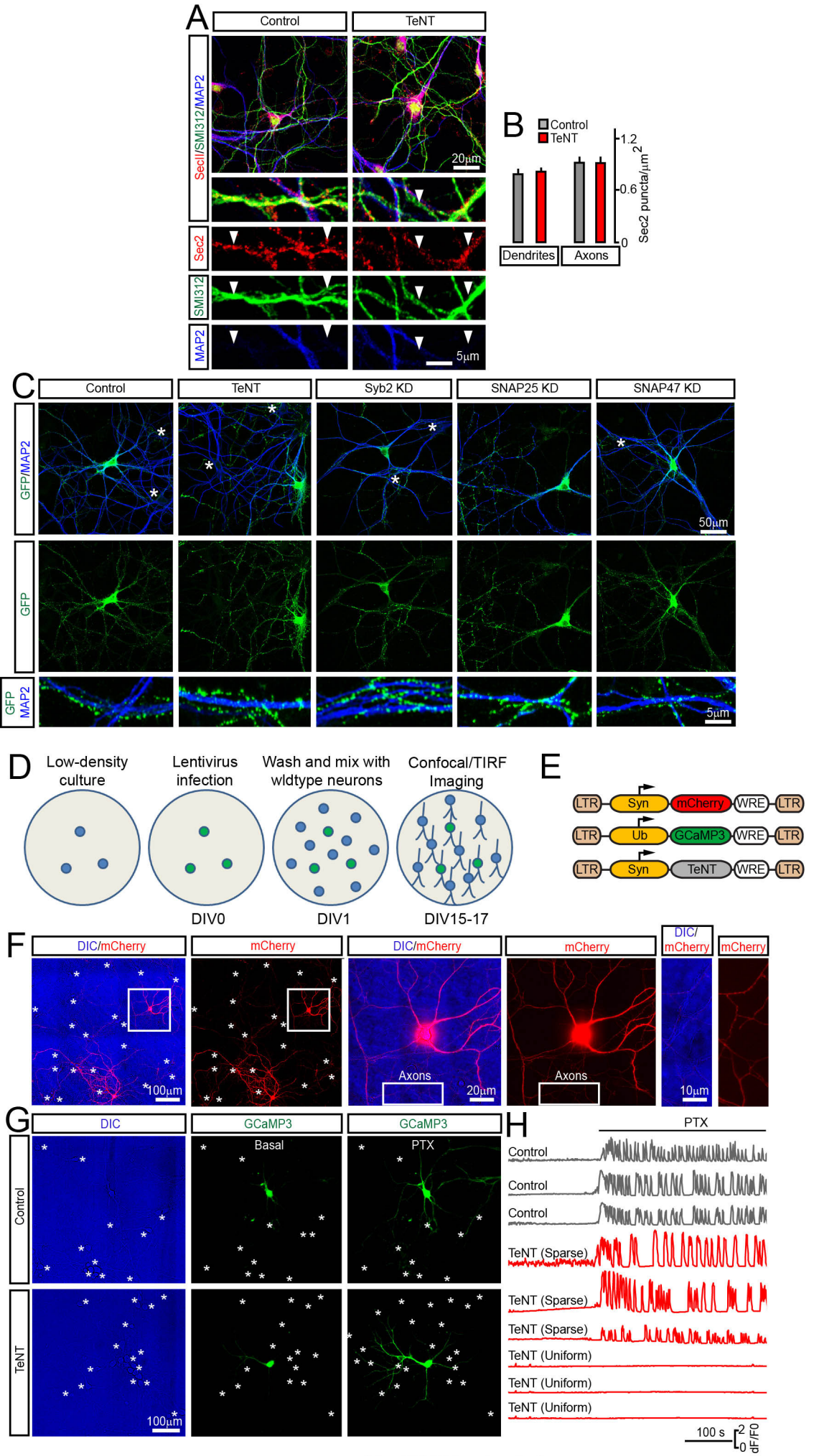

Fig. S3 Shimojo et al

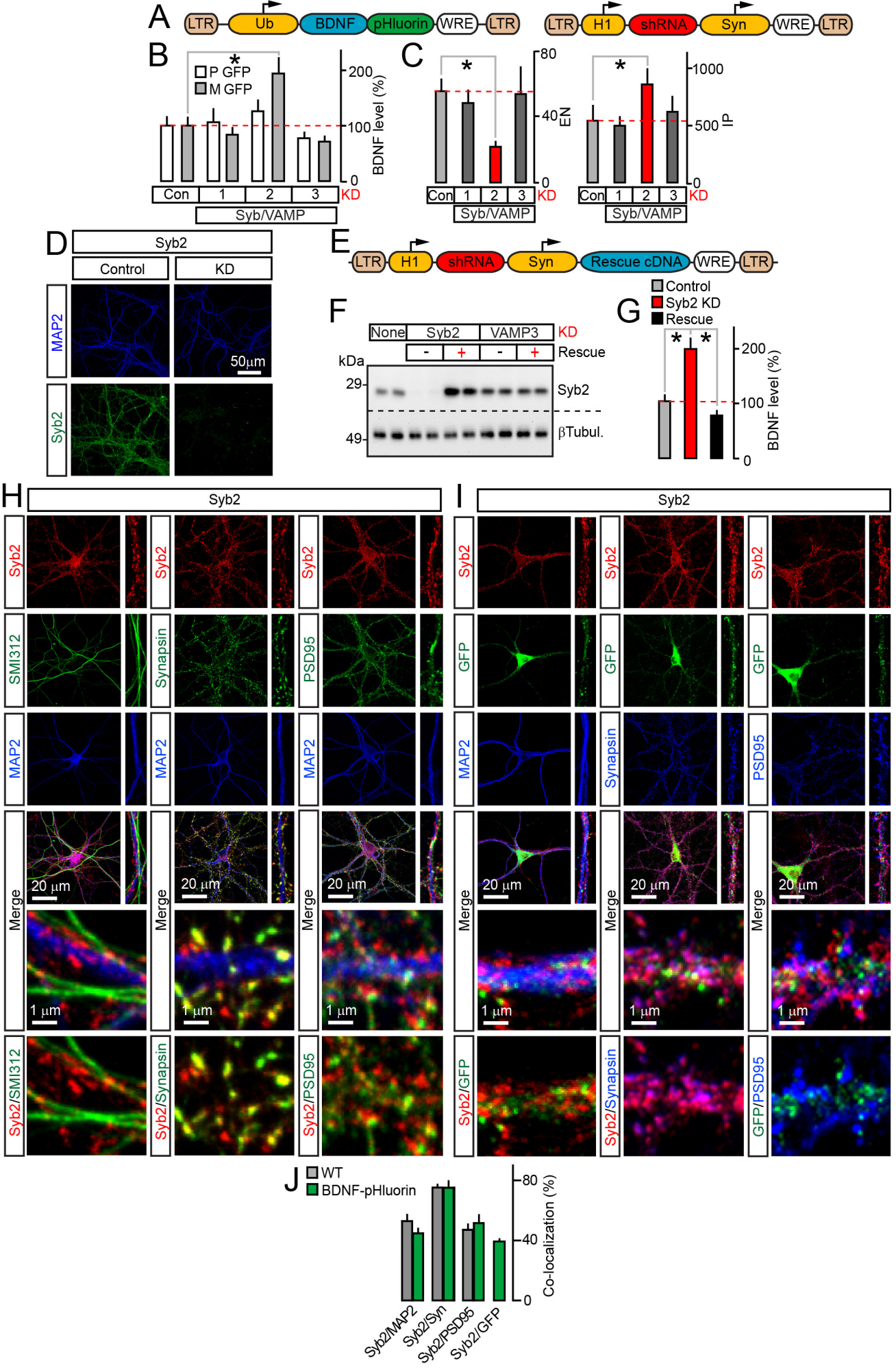

Fig. S4 Shimojo et al

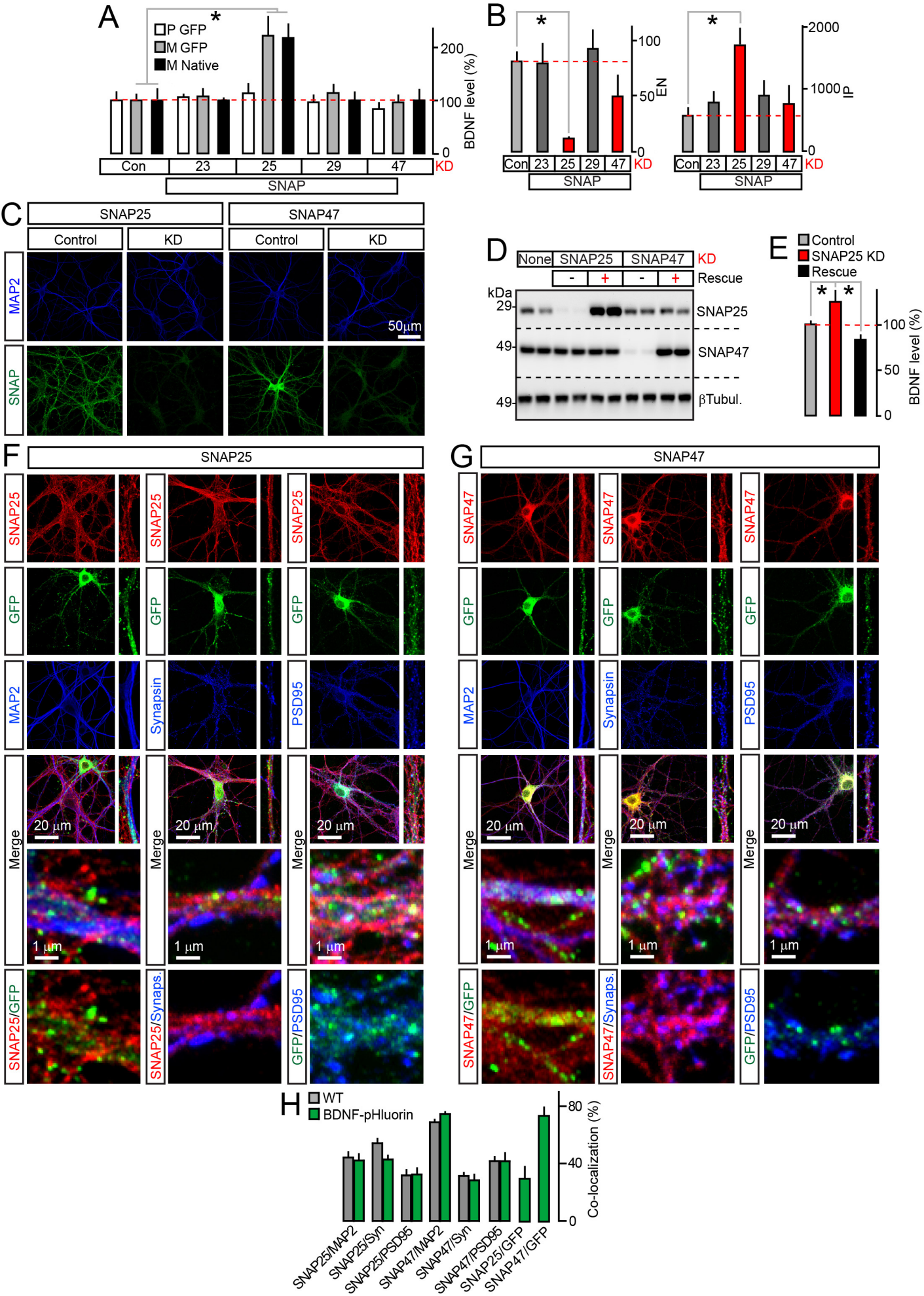

Fig. S5 Shimojo et al

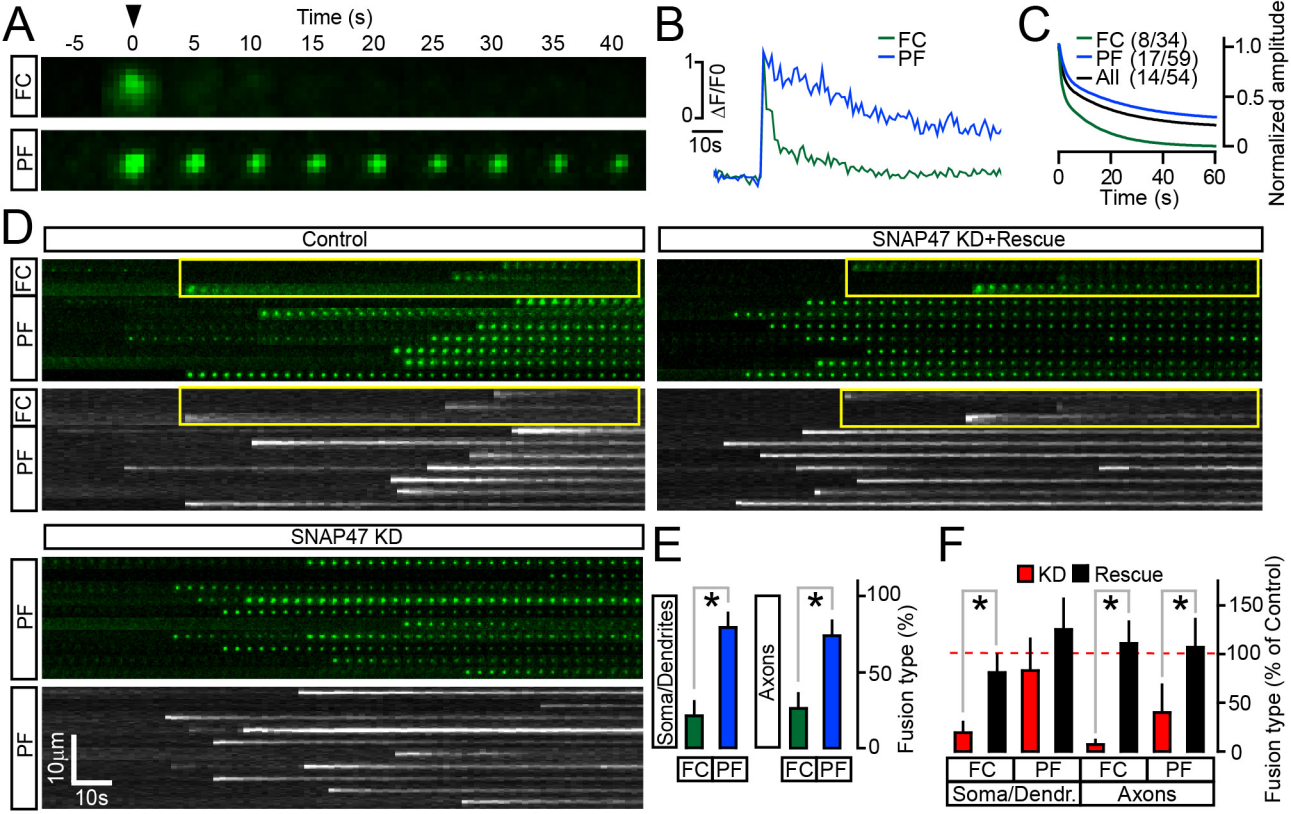

Fig. S6 Shimojo et al

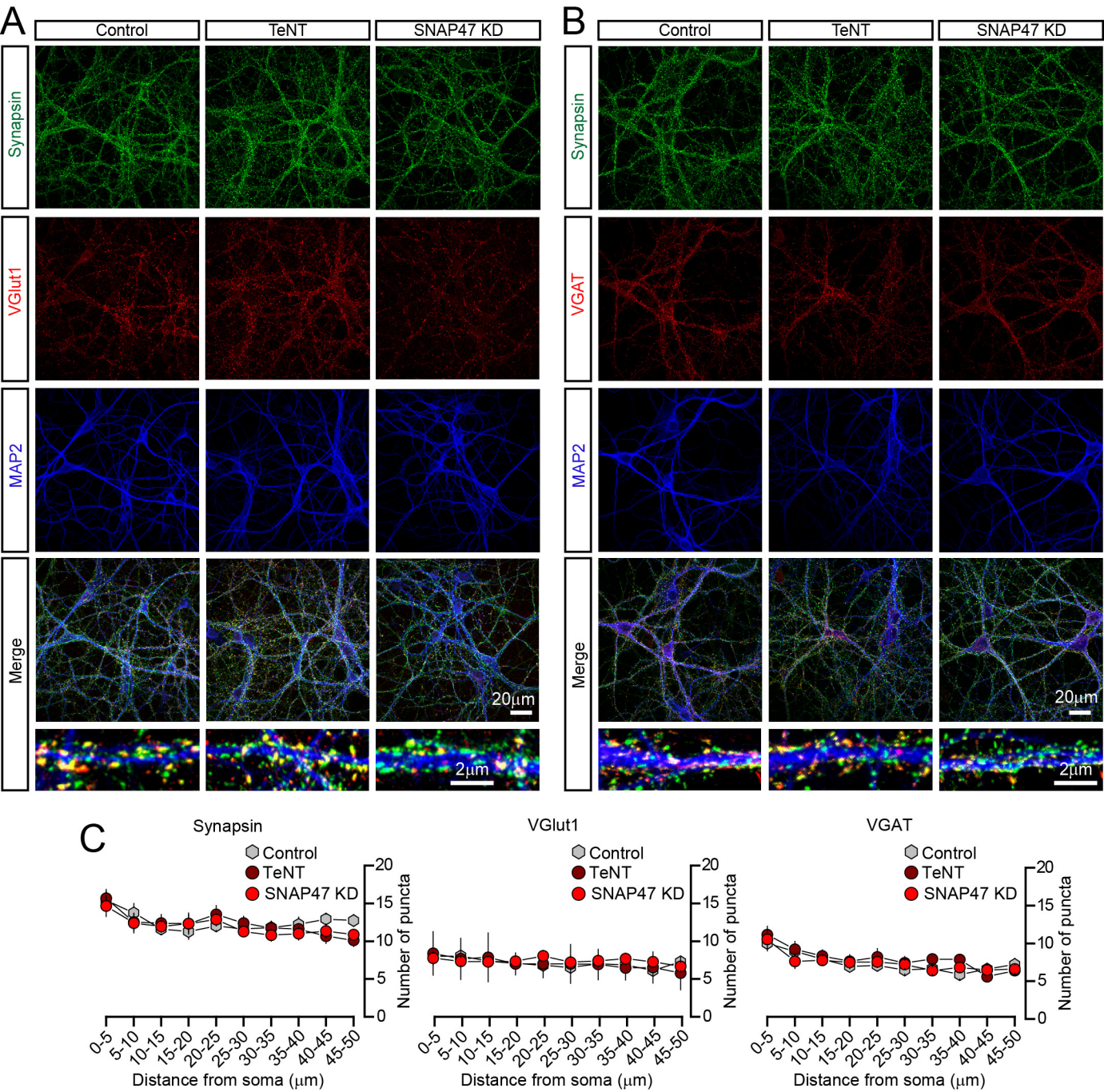

Fig. S7 Shimojo et al

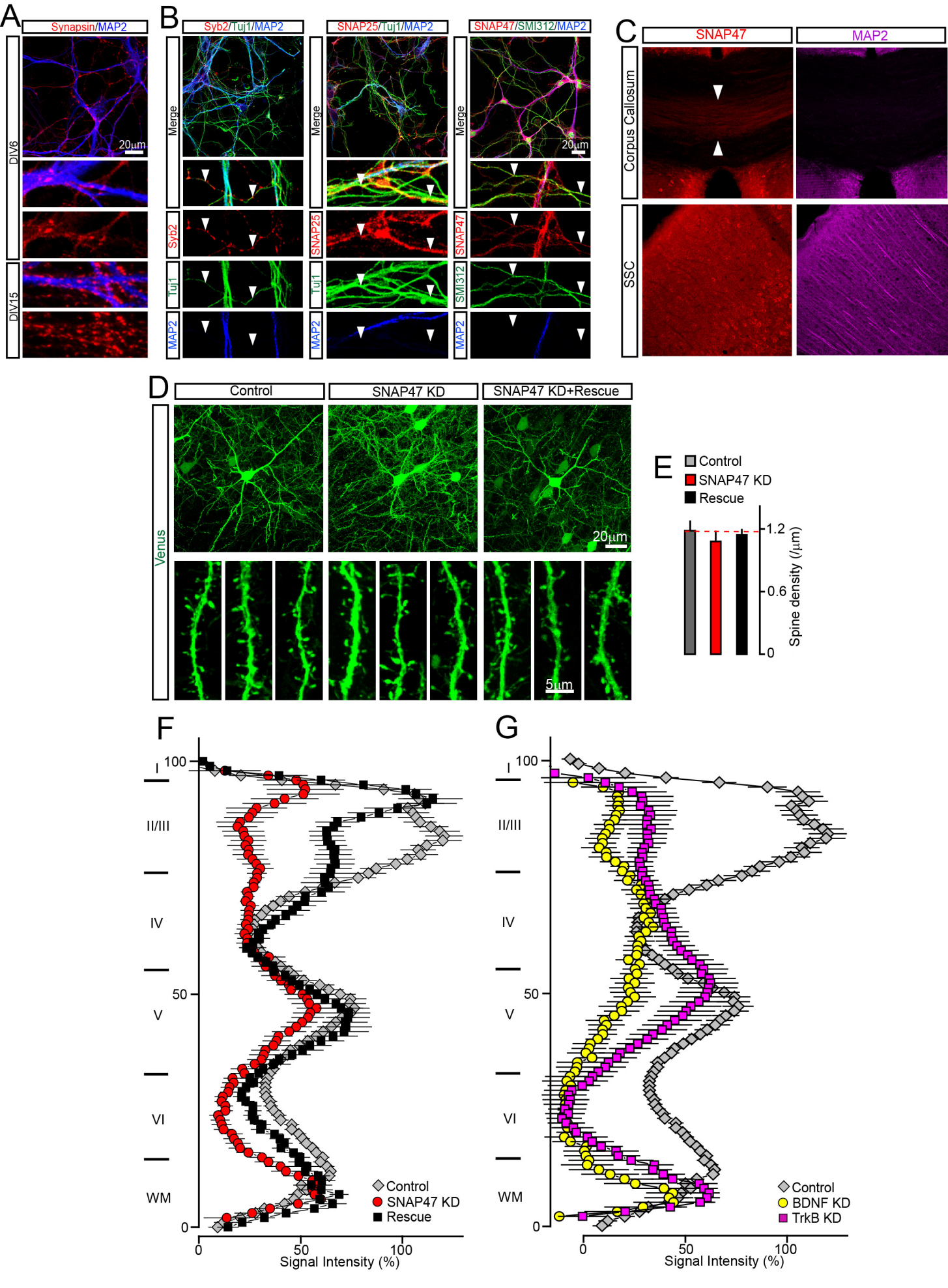

Fig. S8 Shimojo et al